ON THE IMF IN A TRIGGERED STAR FORMATION CONTEXT

The Astrophysical Journal, 808:10 (7pp), 2015 July 20 doi:10.1088/0004-637X/808/1/10

ON THE IMF IN A TRIGGERED STAR FORMATION CONTEXT

Tingtao Zhou[1,2], Chelsea X. Huang[1,3], D. N. C. Lin[1,4,5,6], Matthias Gritschneder[4,7], and Herbert Lau[8]
[1] Kavli Institute for Astronomy & Astrophysics and School of Physics, Peking University, Beijing, China; edmondztt@gmail.com
[2] Department of Physics, Massachusetts Institute of Technology, USA
[3] Department of Astrophysical Sciences, Princeton University, USA
[4] UCO/Lick Observatory, University of California, USA
[5] Institute for Advanced Studies, Tsinghua University, Beijing, China
[6] National Astronomical Observatory of China, Beijing, China
[7] University Observatory Munich, Germany
[8] Argelander Institute, University of Bonn, Germany
Received 2013 May 11; accepted 2015 May 19; published 2015 July 14

ABSTRACT

The origin of the stellar initial mass function (IMF) is a fundamental issue in the theory of star formation. It is generally fit with a composite power law. Some clues on the progenitors can be found in dense starless cores that have a core mass function (CMF) with a similar shape. In the low-mass end, these mass functions increase with mass, albeit the sample may be somewhat incomplete; in the high-mass end, the mass functions decrease with mass. There is an offset in the turn-over mass between the two mass distributions. The stellar mass for the IMF peak is lower than the corresponding core mass for the CMF peak in the Pipe Nebula by about a factor of three. Smaller offsets are found between the IMF and the CMFs in other nebulae. We suggest that the offset is likely induced during a starburst episode of global star formation which is triggered by the formation of a few O/B stars in the multi-phase media, which naturally emerged through the onset of thermal instability in the cloud-core formation process. We consider the scenario that the ignition of a few massive stars photoionizes the warm medium between the cores, increases the external pressure, reduces their Bonnor–Ebert mass, and triggers the collapse of some previously stable cores. We quantitatively reproduce the IMF in the low-mass end with the assumption of additional rotational fragmentation.

Key words: ISM: clouds – ISM: individual objects (Pipe Nebula) – ISM: structure – H II regions – methods: analytical – stars: formation

1. INTRODUCTION

Recent infrared measurements of dust extinction, as well as CO and NH_3 maps of the filaments in molecular clouds, reveal a population of embedded cores mostly confined by the global external pressure from the inter-core gas. These cores are closely associated with the progenitors of young stellar objects. In such filaments, there are gravitationally bound cores (or pre-stellar cores) and embedded protostars (André et al. 2010). However, in the Pipe Nebula, nearly all the cores are starless (Lada et al. 2008). Only the most massive cores in Pipe are gravitationally bound and might collapse. The shape of the core mass function (CMF) of these dense cores (Lada et al. 2008) appears to be qualitatively similar to the broken power law of the stellar initial mass function (IMF; Kroupa 2002; Weidner et al. 2011). An in-depth analysis of their structure and evolution may be useful for the construction of a star formation theory.

One noticeable difference between the CMF and the IMF is an offset between the two distributions. The ratio of the characteristic mass of the IMF over the characteristic mass of the CMF is generally smaller than unity. This ratio ranges from ∼1:3 in the Pipe Nebula (Rathborne et al. 2009) to >1:2 in the Orion (Nutter & Ward-Thompson 2007) and Aquila Nebulae (Könyves et al. 2010). Rathborne et al. (2009) proposed that this offset is due to a direct one-to-one mapping from the cores to the stars with a sufficient amount of mass loss during the star formation process. It is hard to explain in this scenario how the low-mass stars are produced by the originally stable low-mass cores.

Many studies modeling the origin of IMF highlight factors such as the accretion rate of protostars, turbulent fragmentation, and the accretion of cores (see, e.g., Bonnell & Bate 2006; Clark et al. 2008; Anathpindika 2011). In the meantime, constraints such as the small age spread of stars in young clusters are inconsistent in these models.

We propose a scenario to explain the transition from the CMF to the IMF, as well as synchronized star formation, triggered by a few of the first formed O/B stars in the nebula. Many authors (e.g., Strömgren 1939; Spitzer 1978) studied the effects of UV radiation from massive stars on the surrounding regions. The UV radiation generates a hot ionized region (Strömgren sphere), increasing the ambient pressure. Consequently, an isothermal shock is driven through the nebula. Influenced by the Strömgren sphere, denser sub-structures are rapidly enhanced and most of the pre-existing pressure-confined cores are compressed (e.g., Gritschneder et al. 2009). The ionization timescale is generally short compared to the hydrodynamical timescales, such that the increase in the background pressure and temperature can be considered instant in most cases.

In this work, we develop a quantitative understanding of the consequences of this sudden change in the ambient pressure and temperature in the context of the transition from the CMF to the IMF. A direct result is the reduction of the critical Bonnor–Ebert mass (Ebert 1955; Bonnor 1956), making previously unbound cores gravitationally unstable. Therefore, the whole region experiences rapid starburst synchronizing star formation. The shifted Bonnor–Ebert mass also naturally leads to the transition from the CMF distribution to the IMF distribution.

We base our calculations on a Pipe-like cloud with a starless CMF as the starting point of the evolution. We investigated the

formation of a starless CMF in our previous work (Huang et al. 2013, hereafter H13). In H13, we suggest that prior to the onset of global star formation, the cores and the inter-core gas are two separate phases in pressure equilibrium which may result from thermal instability (Lin & Murray 2000). The dynamics of coagulation (Murray & Lin 1996) and ablation (Murray et al. 1993) dominate the evolution of the system, and the star formation timescale is prolonged by the turbulent pressure or magnetic pressure inside the cloud (Lazarian & Vishniac 1999).

In this paper, we consider the consequences of the ignition of the first massive stars in a starless nebula. In Section 2, we suggest that the photoionization of the inter-cloud gas leads to a decrease in the critical Bonnor–Ebert mass and triggers a global burst of star formation. We use this reduced critical mass and the starless CMF from the Pipe to obtain the transition to a stellar IMF in Section 3. We assume different star formation statistics, showing that uncertainties such as binary mass ratio distribution do not affect the IMF shape in a certain parameter range. The discussion and conclusions are presented in Section 4.

2. TRIGGERED STAR FORMATION

After the formation of the first massive stars, their stellar luminosity has a significant influence on the subsequent evolution of the surrounding media. In the presence of a strong UV flux from nearby O/B stars, the diffuse neutral medium, originally at 100 K, hereafter referred to as the warm medium, would be ionized and heated up, while the dense molecular region, originally at 10 K, hereafter referred to as the cold medium, would still be mostly shielded. The resulting increase in the external pressure leads to a reduction in the Bonnor–Ebert mass of the cold cores and a decrease in the star formation timescale.

2.1. The Ionization of the Warm Medium

The ionizing photons from the native stars create Strömgren spheres in the surrounding warm medium. For a typical O/B star with an effective UV photon ($E_\gamma > 13.6$ eV) emission rate of $Q_0 \sim 10^{48-49}$ s^{-1}, the Strömgren radius R_S is determined by

$$Q_0 \sim \frac{4\pi}{3} R_S^3 \, \alpha_B \, n_{\rm warm}^2, \quad (1)$$

where $\alpha_B = 2.6 \times 10^{-13} \, T_4^{0.833-0.034 \log T_4}$ cm^3 s^{-1} is the recombination coefficient (Draine 2011). We define T_4 as the temperature of the warm medium in units of 10^4 K, $Q_{0,49}$ as the number of UV photons in units of 10^{49} s^{-1}, and $n_{\rm warm,2}$ as the warm medium hydrogen number density in units of 10^2 cm^{-3}. Within $R_S \sim 3$ pc $Q_{0,49}^{\frac{1}{3}} \, n_{\rm warm,2}^{-\frac{2}{3}}$ of the ionizing sources, the warm medium is nearly fully ionized with $T_{\rm warm} \sim 10^4$ K. This new temperature corresponds to an increase by a factor of 10–100.

More realistic calculations of equilibrium temperature have been performed with version 08.00 of CLOUDY (last described by Ferland et al. 1998). The effective temperature of the central star is taken to be 34,700 K with a surface luminosity of $\log(L/L_\odot) = 5.59$. This is a typical value for a main-sequence star with a mass of 40 $M_\odot$, produced with the Cambridge stellar evolution code STARS (Eggleton 1971). Assuming a blackbody, the star emits 31% of its power in hydrogen ionization photons, corresponding to $Q_{0,49} \sim 1$.

We assume a solar metallicity for the gas and a standard dust composition. We use a constant hydrogen density of $n_{\rm H} = 774$ cm^{-3} to simulate the warm medium in the Pipe Nebula, to be consistent with the values in Gritschneder & Lin (2012).

The results show that there is a sharp temperature dropoff from several thousand degrees to several hundred degrees at a particular depth of the cloud. The solid line in Figure 1(a) shows the temperature of the warm medium versus the distance from the star. This indicates that the Strömgren radius is 0.7 pc and the temperature inside the ionized sphere is around 9000 K. Given the typical size of a nebula, which is usually a few parsecs, only a few massive stars are needed to ionize most of the inter-core media, leading to a much higher exterior pressure.

2.2. Heating of the Cold Cores

The ionizing UV flux can also penetrate into dense cores. We first consider the heating from the radiation which balances the cooling from recombination.

We denote $R_{\rm ion}$ as the distance from an O/B star at which a typical cold core is heated by the external radiation to 100 K. By neglecting the loss of ionizing photons from the star through the warm medium, we estimate $R_{\rm ion}$ from

$$\frac{R_{\rm ion}}{0.7 \text{ pc}} \sim \left(\frac{Q}{10^{49} \text{ s}^{-1}}\right)^{\frac{1}{2}} \left(\frac{r_c}{0.1 \text{ pc}}\right)^{-\frac{1}{2}} \left(\frac{n_c}{10^4 \text{ cm}^{-3}}\right)^{-1} \times \left(\frac{T_c}{100 \text{ K}}\right)^{-0.5}, \quad (2)$$

where

$$Q_0 \frac{\pi \, r_c^2}{4\pi \, R_{\rm ion}^2} \sim \frac{4\pi}{3} \, r_c^3 \, \alpha_B \, n_{\rm cold}^2, \quad (3)$$

with α_B here being the same as in Section 2.1.

More realistically, we compute the ionization in the cold core with CLOUDY, using the same setup as in Section 2.1, but this time with an initial hydrogen density $n_{\rm H} = 774$ cm^{-3} in the range of $0 \sim 0.5$ pc, while $n_{\rm H} = 7300$ cm^{-3} from 0.5 pc to far away, corresponding to the cold medium placed 0.5 pc from the central star, and the warm medium filling the space in between. Then instead of keeping constant density, we keep the two media in pressure equilibrium as the central star illuminates its surroundings. In this case, the density of the cold medium is enhanced rapidly due to the sudden increase of warm medium temperature and pressure. After the attenuation of the warm medium, the typical photon penetration depth inside the cold medium is only about 0.02 pc. This is much smaller than the typical core radius $r_c \approx 0.1$ pc. Therefore, only cores very near the massive star or very small cores are subjected to this effect. The temperature inside the cores further away is limited by the cooling process to be around 15–20 K, which is two times higher than before the ignition of the UV flux (see Figure 1(b), for depth > 0.5 pc).

In addition, we also investigate the classical evaporation of cores due to the high-temperature environment. Using the formula for the evaporation rate of clouds embedded in a 10^4 K gas (Graham & Langer 1973; Cowie & McKee 1977; McKee &

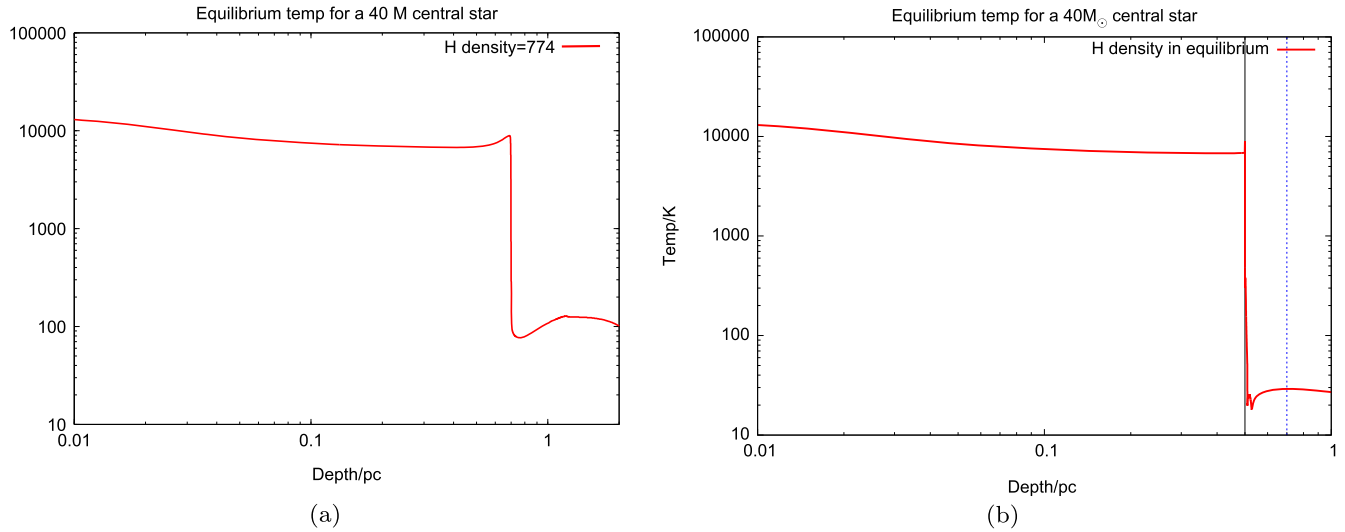

Figure 1. Resulting temperature profiles in the surrounding of a 40 $M_{\odot}$ star for different gas profiles. (a) The red line displays the temperature profile in a medium with constant density $n_0 = 774$ cm^{-3}. The transition from the ionized to the un-ionized medium happens at 0.7 pc (the Strömgen radius). (b) This setup represents a cold core at a distance of 0.6 pc from the central star. The initial density profile is set to $n_0 = 774$ cm^{-3} (inter-core medium) inside 0.5 pc and $n_0 = 7300$ cm^{-3} (core medium) beyond 0.5 pc. The solid vertical line indicates the inner side boundary of the core, i.e., the location of the density jump. The dashed vertical line indicates the extent of the core from the solid vertical line. For computational simplicity, we do not calculate the region behind the core, as the focus of this work lies on the penetration depth at the front side.

Cowie 1977) with the limitations that the background gas is either fully ionized or neutral,

$$\dot{m} = \frac{16\pi\mu\kappa\, r_{\rm c}}{25\, k} = \begin{cases} 1.3 \times 10^{15}\, T^{1/2}\, r_{\rm c,pc}\ {\rm g\ s^{-1}}, & \kappa = \kappa_{\rm n}, \\ 2.75 \times 10^{4}\, T^{5/2}\, r_{\rm c,pc}\ {\rm g\ s^{-1}}, & \kappa = \kappa_{c}. \end{cases} \quad (4)$$

Here, T is the environment temperature, k is the Boltzmann's constant, $r_{\rm c,pc}$ is the radius of the core in units of parsecs, $\kappa_{\rm n}$ is the neutral conductivity, and $\kappa_{\rm c}$ is the classical conductivity for a fully ionized gas.[9] For a typical core with mass $m_{\rm c}$, the evaporation timescale is therefore $\tau_{\rm evap,n} = m_{\rm c}(\dot{m})^{-1} = 8 \times 10^5\, r_{\rm c,pc}^2$ Myr in the neutral case and $\tau_{\rm evap,i} = 4 \times 10^8\, r_{\rm c,pc}^2$ Myr in the fully ionized case. Based on these calculations, the classical evaporation only affects cores with radii as small as 0.01 pc.

We conclude from the above calculation that the evaporation effect is negligible. This is understandable as both the recombination timescale and cooling timescale inside the cold medium are much shorter than these timescales inside the warm gas due to their density contrast. Therefore, the ionization fraction and temperature of the cold medium can be maintained at low levels. We do not include the change of the IMF due to the evaporation in the calculation below.

2.3. Change in Bonnor–Ebert Mass and Star Formation Timescale

The star formation timescale in general can be as long as 100 Myr (Ostriker 2011). However, the collapse process is sped up considerably by the compression of the dense cores due to the UV feedback (Gritschneder et al. 2009). More importantly, the enhancement of the external pressure reduces the Bonnor–Ebert mass and induces the formation of low-mass stars.

The Bonnor–Ebert mass of a cold core can be expressed as $m_{\rm BE} \propto P_{\rm ext}^{-0.5} T_{\rm int}^2$, where $P_{\rm ext}$ is the external pressure (see also Equation (4) in Lada et al. 2008). Prior to the formation of a massive star, the temperature of the warm medium is $T_{\rm ext} \sim 100$ K, and the cores' temperature is $T_{\rm int} \sim 10$ K. In pressure equilibrium, the density contrast between the cores and medium is ~10. The influx of the UV photons from an emerging massive star ionizes the tenuous warm medium within 1 pc from the star and raises the medium's temperature to $T_{\rm ext} \sim 9000$ K. In contrast, the temperature within the cores remains at $T_{\rm int} \sim 20$ K (see Figure 1).

The ionization front propagates through the warm medium more rapidly than the sound speed. Consequently, the increase in $T_{\rm ext}$ leads to an increase in $P_{\rm ext}$ by a similar factor before the medium's density can readjust to a new pressure equilibrium. Due to the combined effect of the temperature and pressure increase in both the warm medium and the cold medium, the Bonnor–Ebert mass decreases by a factor of 2.38, shifting from around 2 $M_{\odot}$ (Lada et al. 2008) to 0.84 $M_{\odot}$ in our model.

Due to this sudden increase of the external pressure, global, coordinated star formation is induced, leading to a starburst. Several factors may introduce some dispersions into the value of the modified $m_{\rm BE}$. For example, the flux of ionizing photons emitted by the first O/B star would be reduced by an order of magnitude if its mass were halved (the one we have considered in Figure 1 is 40 $M_{\odot}$). Nevertheless, the final temperature of the ionized region and the core only changes slightly. The Bonnor–Ebert mass associated with slightly lower $T_{\rm ext}$ (8500 K) and $T_{\rm int}$ (15 K) would reduce $m_{\rm BE}$ to 0.47 $M_{\odot}$. In this case, the Strömgren sphere around the star will be much smaller, which would slow down the global star formation process and extend the age spread in this nebula. If the global star formation timescale is comparable or longer than the timescale of core coagulation, the dynamics of cores may affect the IMF further. Here, we neglect this effect on the age spread and the effect from the evolution of cores. Once a core becomes

[9] Note that a different mean molecular weight μ is used for the two cases.

gravitationally unstable, it collapses on a free fall timescale[10]

$$t_{\rm sf} \sim t_{\rm ff} = \sqrt{\frac{r_{\rm c}^3}{G\, m_{\rm c}}} \sim 0.3\ {\rm Myr} \left(\frac{r_{\rm c}}{0.1\ {\rm pc}}\right)^{3/2} \times \left(\frac{m_{\rm c}}{2\ M_\odot}\right)^{-1/2}. \quad (5)$$

This timescale is much shorter than that associated with the dynamical evolution of the dense cores prior to the formation of the first massive stars, which is about 5 Myr from H13. After the external medium is ionized by the first massive stars, the compression of the cores reduces the cross-section and enhances the density contrast between the core and the external medium. This increases both the coagulation and the fragmentation timescales. Therefore, the further dynamical evolution of the CMF can be neglected.

3. FROM THE CMF TO THE IMF

The initial stellar mass function is determined by the induced collapse of the dense cores with a preset CMF. The calculations presented here follow our previous work on the CMF (H13). In the previous paper, we discussed the evolution of the dense core mass distribution with a modified coagulation equation. The CMF acquires a stable shape which resembles a typical observed CMF after several million years of evolution time. During this stage, prior to the triggered star formation we discuss here, a typical star formation timescale is around 100 Myr, which retains the starless nature of the system. Figure 2(a) shows the pre-stellar core mass distribution compared with the Chabrier System IMF (Chabrier 2003) and recent observations (Rathborne et al. 2009). The intermediate-mass range of the CMF (0.3–0.5 $M_\odot$) can also be parameterized with similar two power-law slopes as the Kroupa IMF, only shifted to a higher mass range by a factor of about three (Lada et al. 2008). We note that both the observed CMF and modeled CMF have a slightly steeper slope than the IMF at the high-mass end. However, the uncertainty is also higher in those bins due to the small number statistics. We now take the modeled CMF (H13) as the initial condition and assume the global star formation is triggered simultaneously. During a time step δt, the number of stars in the mass range $m \sim m + dm$ increases by

$$\frac{\Delta n^*\left(m^*\right)}{\Delta t} = \int_{m_{\rm min}}^{m_{\rm max}} m_{\rm c} n(m_{\rm c}) \eta_{\rm sf} \gamma_{\rm sf} \frac{P\left(m_{\rm c}, m^*\right)}{m^*}\, dm_{\rm c}, \quad (6)$$

where $n(m_{\rm c})$ is the number density of cores within the mass interval $(m_{\rm c}, m_{\rm c} + dm_{\rm c})$, $\eta_{\rm sf}(m_{\rm c})$ is the retention factor (see Section 3.1), $\gamma_{\rm sf}(m_{\rm c})$ is the star formation rate for a dense core with mass $m_{\rm c}$, and $P(m_{\rm c}, m^*)$ is the percentage of the core mass $(m_{\rm c})$ transferred into this specific star mass (m^*) bin.

The real star formation process may depend on the different initial conditions of the progenitor cores. Here, we present several limiting cases. To quantify our results, we fit our computed IMFs with a Chabrier-like function $\phi(\mu, \sigma, m_0, \gamma)$, where m_0 is the transition mass separating the two parts of the piece-wise Chabrier-like function. For masses smaller than m_0, the model IMF is described by a lognormal form with a mean around μ and dispersion σ; meanwhile, the distribution at masses larger than m_0 is described by a power law with index γ. We require the distribution to be continuous at m_0. The best-fitting parameters are shown in Table 1. We compare these fits with the Chabrier IMF (Chabrier 2003) model and discuss the limits of different prescriptions.

3.1. Case 1: Burst of Single Stars

Given the similarity between the CMF and the IMF, some authors suggested a one-to-one conversion of dense cores into young stars (e.g., Lada et al. 2008). Although this scenario has been criticized on the basis of binary stars' prevalence (see, e.g., Smith et al. 2009), it is nonetheless informative to explore this simplest possibility. In this case, $P(m_{\rm c}, m^*) = \delta(m^* - m_{\rm c}\eta_{\rm sf}(m_{\rm c}))$ (see Equation (6)). $\eta_{\rm sf}$ is the retention factor, which is the fraction of core mass finally remaining in the stars, for one particular core, while the more often loosely used phrase "star formation efficiency" should refer to the global ratio of total stellar masses over total progenitor core masses in a certain region and timescale. In Figure 2(b), we show the IMFs generated with this model. We assume only cores with masses exceeding the Bonnor–Ebert mass can form stars, such that the star formation rate

$$\gamma_{\rm sf}(m_{\rm c}) = \begin{cases} 0 & \text{if } m_{\rm c} < m_{\rm BE}, \\ \Gamma_{\rm sf} & \text{if } m_{\rm c} \geqslant m_{\rm BE}. \end{cases} \quad (7)$$

Here, $\Gamma_{\rm sf} = t_{\rm sf}^{-1}$ (see Equation (5)) is the characteristic star formation rate. We also assume that the retention factor, i.e., the amount of the core mass retained in the resulting star, is constant with a value $0 < \eta_{\rm sf}(m_{\rm c}) < 1$.

The results in Figure 2(b) show that the IMFs are shifted toward the low-mass end with a broad peak near the original Bonnor–Ebert mass modified by the retention factor. With $\eta_{\rm sf} = 0.3$, the new peak is around 0.7 $M_\odot$, which corresponds to Lada's suggestion (Lada et al. 2008). The overall shape of the IMF resembles the observed stellar IMF. The low-mass end has a similar dispersion to that of Chabrier's IMF, provided the retention factor $\eta_{\rm sf}$ is not a sensitive function of the progenitor core mass. The high-mass end power law is steeper than the Salpeter slope (Salpeter 1955), where the observational uncertainty in this range is also relatively large. However, the minimum mass of stars we can produce with a single star formation prescript is dependent on the critical Bonnor–Ebert mass and $\eta_{\rm sf}$ such that $m_{\rm cut\text{-}off} \sim m_{\rm BE,new}\eta_{\rm sf}$. Due to this cut-off, even with a low value of $\eta_{\rm sf}$ ($\eta_{\rm sf} = 0.3$, dark gray line in Figure 2(b)), this model has no inference for the lowest-mass stars. The bulk of the modeled IMFs are more massive than the Chabrier IMF. We conclude that a non-unity retention factor alone would not explain the transition from CMF to IMF.

3.2. Case 2: Solely Binary Formation

A large fraction of the young stars are binaries. Each component of the binary contributes to the statistics of the IMF. Another limiting case of interest is the possibility that all the cores with masses in excess of the modified Bonnor–Ebert mass would fragment into binary stars. In principle, binary star

[10] Note that after the collapse the accretion flow onto the cores could be still active and the star formation process may continue. Here, we are mainly concerned with the epoch before stellar feedback is activated. The star formation timescale $t_{\rm sf}$ should still be well approximated with the free fall time $t_{\rm ff}$.

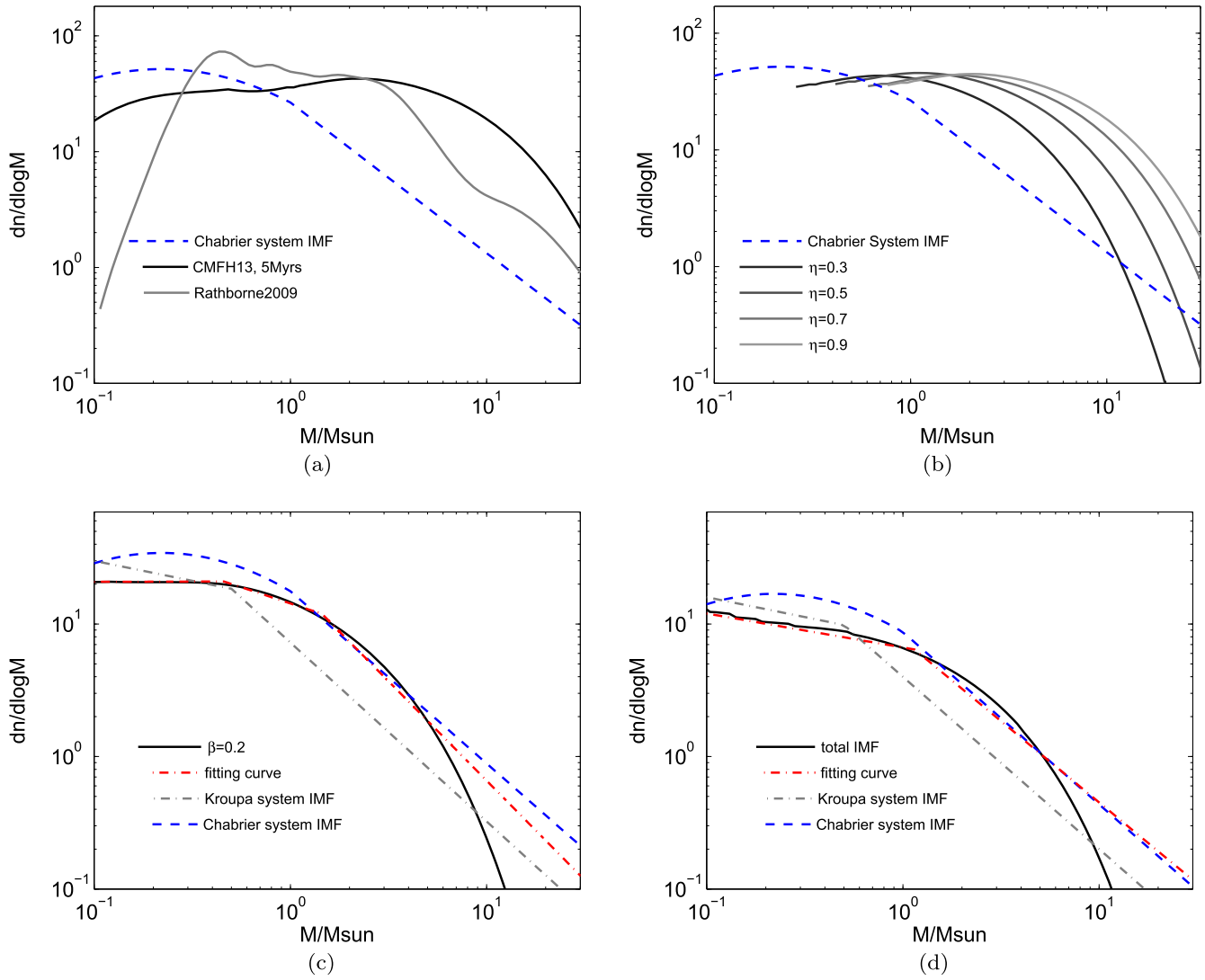

Figure 2. CMFs and IMFs generated in our model under different assumptions. (a) The CMF obtained from H13 (solid black line) is adopted as the initial condition for our calculations. Gray line shows the observed CMF in the Pipe from Rathborne et al. (2009). For comparison, the Chabrier IMF (Chabrier 2003), shifted to the low-mass end by a factor of 3, is shown as the dashed blue line. (b) Gray curves are displaying the stellar IMFs for single stars with different retention factors $\eta_{\rm sf}(m_{\rm c})$. Any core evolution through coagulation or fragmentation is neglected. (c) The black solid line is showing the generated total IMF if all the cores undergo binary fragmentation with $\beta = 0.2$ (see Equation (8)) and $\eta_{\rm sf}(m_{\rm c}) = 0.3$. (d) The black solid line is showing the total IMF, assuming 100% binary star formation. The secondary stellar masses follow a power-law distribution with index $\alpha = 1.5$ (see Equation (9)). We show both the Chabrier IMF (blue dashed curve) and the Kroupa IMF (Kroupa 2002, gray dashed–dotted lines) as a comparison. The modeled IMF is fitted with a broken power law (red dashed–dotted lines).

Table 1
IMF from Different Star Formation Models

Distribution	$\mu(M_\odot)$ Mean	$\sigma(M_\odot)$ Dispersion	$m_0(M_\odot)$ Transition Mass	γ Power-law Index	SSR Sum of Squared Residuals
Chabrier	0.22	0.57	1.00	1.30	N/A
single0.3	0.66	0.54	4.05	2.19	0.000011
single0.5	1.05	0.54	6.42	2.18	0.000011
single0.7	1.55	0.54	9.36	2.14	0.000011
single0.9	1.95	0.55	11.02	1.98	0.0000097

Note. List of parameters for the resulting IMFs modeled with a Chabrier type function. We fitted the resulting IMF in the mass range 0.1–30 $M_\odot$ with $\frac{dn}{d\log m} \propto e^{\frac{-\log(m/\mu)^2}{2\sigma^2}}$ for $m < m_0$, and with $\frac{dn}{d\log m} \propto m^{-\gamma}$ for $m > m_0$. Continuity is imposed at m_0. Columns starting with "single" refer to the results from the single star formation model in Section 3.1, and the number attached to it corresponds to the retention efficiency.

formation is a consequence of rotational fragmentation and the kinematic properties are determined by the angular momentum distribution of the cores and their cooling ability. However, we are primarily interested in the IMF rather than the period distribution. We adopt an idealized power-law distribution for the mass ratio q, such that

$$\frac{dn^*_{\rm binary}}{dq} \propto q^{-\beta}. \quad (8)$$

Here, the cut-off is taken as $q_{\rm min} = 0.05$. We explore a range of power-law indices β between 0.2 and 2.5, which essentially covers the extreme limits. We assume a constant retention $\eta_{\rm sf} = 0.3$ and star formation rate same as in Equation (7). The results here remain valid if the retention factor does not vary strongly with the progenitor core mass.

All the resulting IMFs with different β display a broad shifted peak around the new, reduced Bonnor–Ebert mass

(Figure 2(c)). The results are very slightly affected by different β in this wide range, so only $\beta = 0.2$ is shown. The mass associated with the turn-over of the IMF is smaller than that found for the single star formation model. The segments in 0.46 $M_\odot < m \leqslant 1.45\ M_\odot$ with power-law index $\gamma_1 = 0.489$ and in 1.45 $M_\odot < m \leqslant 10\ M_\odot$ with power-law index $\gamma_2 = 1.5$. The two indices are quite similar to those of the piece-wise Kroupa IMF. We expect that the allowance of trinaries and quaternaries will further move the peak toward the low-mass end.

3.3. Case 3: The Binary Companion's IMF

In a classical study of the binary star population census by Duquennoy & Mayor (1991), the IMF for the companions of G-dwarf stars is thoroughly analyzed. They show that binaries, on average, can be formed by random combination of stars drawn from the same IMF. Following their basic approach, we consider the IMF of the primary and secondary stars separately. We assume all the progenitor cores fragment into binaries and the secondary star masses follow a distribution (e.g., Gaussian, Salpeter, or Miller-Scalo (Miller & Scalo 1979) power law) independent of their primaries' mass. For simplicity, we adopt a power law, so the transfer functions as in Equation (6) become

$$P_{\rm sec}\ (m_{\rm sec}, m_{\rm c}) \propto dn_{\rm sec}/dm_{\rm sec} \propto (m_{\rm sec})^{-\alpha}, \tag{9}$$

$$P_{\rm prim}\,(m_{\rm sec}, m_{\rm c}) = P_{\rm sec}\ (\eta m_{\rm c} - m_{\rm sec}, m_{\rm c}), \tag{10}$$

where the subscripts "sec" and "prim" represent the secondary and primary stars. For $P_{\rm sec}$ the range of m^* is 0.08 $M_\odot < m_{\rm sec} < 0.5\ \eta_{\rm sf} m_{\rm c}$. The power-law index for the secondary star mass distribution, α, varies from 0.8 to 1.5 in our calculations, while the star formation rate is as in Equation (7) and the retention factor $\eta_{\rm sf} = 0.3$ is still assumed. Here, the IMF of the primary star preserves its characteristic broad peak and overall shape. The characteristic mass associated with this peak is smaller than that of the CMF.

The consequent IMF for the primary stars is very slightly influenced by α in this wide range, so we only show the result with $\alpha = 1.5$ in Figure 2(d). Following Duquennoy & Mayor (1991), we compare the total (primary and secondary) simulated IMF with some well-known IMFs, such as the Kroupa IMF. The shape of the modeled IMF resembles the Kroupa IMF more closely at masses below 0.7 $M_\odot$. We fit it with two broken power laws. The low-mass end ($m < 1\ M_\odot$) completely reproduces the assumed power law we put in, with $dn/d\ \log\ m = m^{-0.5}$, while the intermediate mass range ($1\,M_\odot < m < 10\,M_\odot$) recover the Salpeter power law $dn/d\ \log\ m = m^{-1.3}$.

3.4. Analytical Results for the Binary Mass Ratio Distribution

An alternative approach to characterize binary star statistics is to utilize the mass ratio, defined as $q = m_{\rm sec}/m_{\rm prim}$. Observations show that the mass ratio also roughly follows a power-law distribution, as in Scorpius OB2 for intermediate-mass stars (Kouwenhoven et al. 2007). Given a probability distribution of mass ratio $p(q|m_{\rm core})$ in a binary formation process (formed from cores with mass $m_{\rm core}$), we can combine it with the CMF $p(m_{\rm core})$ to predict the mass ratio distribution $f(q)$:

$$p(q) = \int_{m_{\rm min}}^{m_{\rm max}} p\left(q\middle|m_{\rm core}\right) p(m_{\rm core})\, dm_{\rm core}. \tag{11}$$

With a power-law mass distribution of the progenitor dense cores and an assumed constant retention, we can estimate the probability of finding a binary system with stellar masses of $m_{\rm prim}$ and $m_{\rm sec}$ to be

$$f\,(m_{\rm prim}, m_{\rm sec}\,) \propto \left(m_{\rm prim} + m_{\rm sec}\right)^{-\alpha}, \tag{12}$$

where α is the power-law index of the progenitor CMF. For random pairing of binary systems (Duquennoy & Mayor 1991),

$$pq\ |m_{\rm core}) = \frac{1}{1 - q_{\rm min}} \qquad \text{for } q \in \left[q_{\rm min}, 1\right] \tag{13}$$

with $q_{\rm min}$ as the minimum allowed binary ratio.

The cumulative probability $P(q < x)$ for all the binary systems would then be

$$P\,(q < x) = \int_{m_{\rm min}}^{x m_{\rm max}} dm_{\rm prim} \times \int_{\frac{m_{\rm prim}}{x}}^{m_{\rm max}} dm_{\rm sec} f\,(m_{\rm prim}, m_{\rm sec}\,). \tag{14}$$

Thus, the statistically averaged distribution of mass ratios q would be

$$f\,(q) \equiv \frac{dP(q)}{dq} \propto \frac{1 + (2 - \alpha)q + (1 - \alpha)q_{\rm min}^{2-\alpha} q^{\alpha-2}}{(2 - \alpha)(1 + q)^{\alpha}} - (1 + q)^{1-\alpha}, \tag{15}$$

where $m_{\rm max}$ ($= \eta_{\rm sf} m_{\rm core}$) is the upper limit for progenitor core mass. We choose α values corresponding to Kroupa's IMF power-law indices. Although there are some uncertainties in the minimum allowed mass ratio, binary systems with a q ratio around 0.05 or less have been observed so we adopt $q_{\rm min} = 0.05$ in the calculation. Results are shown in Figure 3 and compared with the observed power law from Kouwenhoven et al. (2007). Although the distribution of q depends on the value of $q_{\rm min}$, the power-law slope converges, for $q \gg 0.05$, to the observed value.

4. DISCUSSION AND CONCLUSIONS

In this work, we continue our investigation on the origin of the stellar IMF. Based on the similarity between the observed stellar IMF and the CMF of dense starless cores in the Pipe Nebula, we assume that they are closely connected. In Gritschneder & Lin (2012), we suggest that the cold cores of molecular gas are the byproducts of a thermal instability or the fragmentation of the shocked shell, and that they are pressure confined by tenuous warm atomic medium. The CMF of these cores is the natural outcome of their collisional coagulation and their fragmentation due to their hydrodynamic interaction with the surrounding medium (H13). We also assume that these cores become unstable, undergo gravitational collapse, and evolve into protostars after their mass exceeds the Bonnor–Ebert mass.

Although this simple model reproduces the basic observed slopes of the stellar IMF, there is a factor of three offset

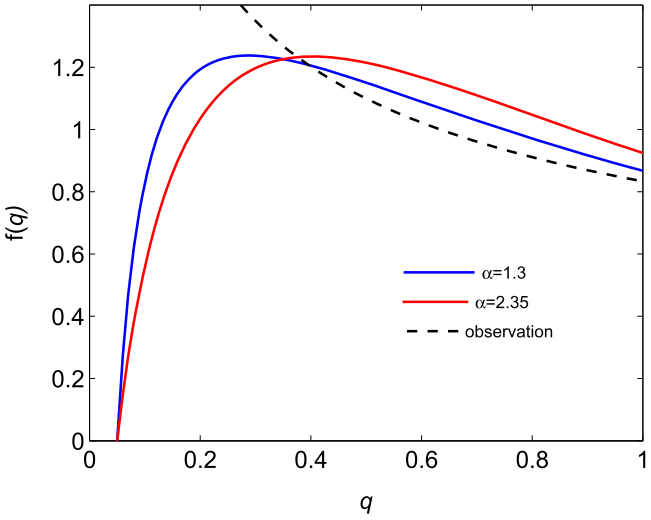

Figure 3. Analytical results for $f(q)$, i.e., the probability distribution function (PDF) of observed mass ratios ($q = m_{\rm sec}/m_{\rm prim}$) in binary systems. The conditional distribution of mass ratio given the progenitor core mass is assumed to be a uniform distribution in ($q_{\rm min}$, 1) regardless of $m_{\rm core}$ (see Equation (13)). For the CMF prescription $dn/dm = m^{-\alpha}$, the blue line corresponds to $\alpha = 1.3$ and the red line corresponds to $\alpha = 2.35$. The total accumulated probability is renormalized to 1 and $q_{\rm min} = 0.05$. The dashed line is the best fit power law ($f(q) \propto q^{-0.4}$) to the observations from Kouwenhoven et al. (2007).

between the stellar mass associated with the peak of the stellar IMF and that associated with the peak of the cores' CMF. The main motivation of the investigation presented in this paper is to suggest a mechanism to account for this shift.

In Huang et al. (2013), we suggested that the peak of the CMF is essentially the Bonnor–Ebert mass of the cores. In typical molecular clouds, such as the Pipe Nebula, the Bonnor–Ebert mass is >1 $M_{\odot}$. In principle, cores less massive than the Bonnor–Ebert mass are stable and do not turn into stars. Yet, many low-mass stars are formed in young stellar clusters.

In this work, we make an attempt to resolve the issues of (1) the offset between the mass associated with the peak of the CMF and the IMF and (2) the prolific production of sub-solar type stars in molecular clouds. We demonstrate that the onset of first massive stars in these clouds photoionize and heat the surrounding medium without significantly changing the ionization fraction and temperature of the cores. This feedback effect largely increases the external pressure that confines the cores (by up to two orders of magnitude). This change leads to the compression of the cores and a reduction in their Bonnor–Ebert mass.

The collapse of cores with a mass greater than the modified Bonnor–Ebert mass (and less than the original Bonnor–Ebert mass) can now lead to the formation of a large population of sub-solar-mass stars. The stellar IMF generally preserves the shape of the Salpeter-like CMF with a significant lowering in the peak mass. The shape of the IMF (dispersion and high-mass end slope) is not strongly modified by the formation of binary stars through rotational fragmentation. In our model, the inclusion of binary fragmentation during the collapse is essential for the production of stars with mass lower than the modified Bonnor–Ebert mass.

One implication of this induced star formation scenario is that the intrinsic age spread of the stellar cluster is naturally very small. In our analysis, we have adopted an idealized treatment of the retention efficiency (often loosely referred to as star formation efficiency). A mass dependence in the retention factor may lead to some modification in the IMF. We present several models for single and binary star populations. They generally reproduce the transition from the CMF to the IMF suggested by the observational data. A prolific production of triple and hierarchical systems may also lead to the formation of very low-mass stars.

Finally, these models are constructed with solar composition. In metal-deficient gas, such as protoglobular cluster clouds, the inability to cool may lead to a higher internal temperature and a higher Bonnor–Ebert mass in the cores. This feedback mechanism may be particularly important in triggering the formation of low-mass stars with lifespans in excess of 10 Gyr. We will further explore this possibility in the future.

We thank M. B. N. Kouwenhoven and C. Lada for useful conversations. D.N.C.L. acknowledges support by NASA through NNX08AL41G. M.G. acknowledges support from the Humboldt Foundation in form of a Feodor Lynen Fellowship.

REFERENCES

Anathpindika, S. 2011, NewA, 16, 477
André, P., Men'shchikov, A., Bontemps, S., et al. 2010, A&A, 518, L102
Bonnell, I., & Bate, M. 2006, MNRAS, 370, 488
Bonnor, W. B. 1956, MNRAS, 116, 351
Chabrier, G. 2003, PASP, 115, 763
Clark, P., Bonnel, I., & Klessen, R. 2008, MNRAS, 386, 3
Cowie, L. L., & McKee, C. F. 1977, ApJ, 211, 135
Draine, B. T. 2011, Physics of the Interstellar and Intergalactic Medium (Princeton, NJ: Princeton Univ. Press)
Duquennoy, A., & Mayor, M. 1991, A&A, 248, 485
Ebert, R. 1955, ZA, 37, 217
Eggleton, P. P. 1971, MNRAS, 151, 351
Ferland, G. J., Korista, K. T., Verner, D. A., et al. 1998, PASP, 110, 761
Graham, R., & Langer, W. D. 1973, ApJ, 179, 469
Gritschneder, M., & Lin, D. N. C. 2012, ApJL, 754, L13
Gritschneder, M., Naab, T., Burkert, A., et al. 2009, MNRAS, 393, 21
Huang, X., Zhou, T., & Lin, D. N. C. 2013, ApJ, 769, 23
Kouwenhoven, M. B. N., Brown, A. G. A., Portegies Zwart, S. F., et al. 2007, A&A, 474, L77
Könyves, V., André, P., Men'shchikov, A., et al. 2010, A&A, 518, L106
Kroupa, P. 2002, Sci, 295, 82
Lada, C., Muench, A. A., Rathborne, J., et al. 2008, ApJ, 672, 410
Lazarian, A., & Vishniac, E. T. 1999, ApJ, 517, 700
Lin, D. N. C., & Murray, S. D. 2000, ApJ, 540, 170
McKee, C. F., & Cowie, L. L. 1977, ApJ, 215, 213
Miller, G. E., & Scalo, J. M. 1979, ApJS, 41, 513
Murray, S. D., & Lin, D. N. C. 1996, ApJ, 467, 728
Murray, S. D., White, S. D. M., Blondin, J. M., & Lin, D. N. C. 1993, ApJ, 407, 588
Nutter, D., & Ward-Thompson, D. 2007, MNRAS, 374, 1413
Ostriker, E. C. 2011, Computational Star Formation, 270, 467
Rathborne, J. M., Lada, C. J., Muench, A. A., et al. 2009, ApJ, 699, 742
Salpeter, E. E. 1955, ApJ, 121, 161
Smith, R. J., Clark, P. C., & Bonnell, I. A. 2009, MNRAS, 396, 830
Spitzer, L. 1978, Physical Processes in the Interstellar Medium (New York: Wiley-Interscience)
Strömgren, B. 1939, ApJ, 89, 526
Weidner, C., Kroupa, P., & Pflamm-Altenburg, J. 2011, MNRAS, 412, 979